# Von Kármán vortex street in a Bose-Einstein condensate

Kazuki Sasaki, Naoya Suzuki, and Hiroki Saito
*Department of Applied Physics and Chemistry, University of Electro-Communications, Tokyo 182-8585, Japan*
(Dated: February 10, 2010)

Vortex shedding from an obstacle potential moving in a Bose-Einstein condensate is investigated. Long-lived alternately aligned vortex pairs are found to form in the wake, as for the von Kármán vortex street in classical viscous fluids. Various patterns of vortex shedding are systematically studied and the drag force on the obstacle is calculated. It is shown that the phenomenon can be observed in a trapped system.

PACS numbers: 03.75.Kk, 03.75.Lm, 47.32.ck

The formation of a train of alternate vortices in the wake past an obstacle, known as the von Kármán vortex street, is a ubiquitous and intriguing phenomenon in fluids. Since the pioneering experimental study by Bénard [1] and theoretical consideration by von Kármán [2], numerous studies have been made on the phenomena of vortex street formation [3].

The behavior of a viscous fluid flowing past an obstacle is determined by the Reynolds number Re, which is a dimensionless parameter that includes the kinematic viscosity. The wake of a cylinder is steady for Re below around 50, and a vortex street emerges for $10^2 \lesssim \mathrm{Re} \lesssim 10^5$, which becomes turbulence for a larger Re. This implies that the viscosity plays an important role in vortex street formation in classical fluids. For superfluids, however, the Reynolds number cannot be defined because of the absence of viscosity. Moreover, the vortex quantization makes superfluid dynamics quite different from classical fluid dynamics. Therefore, it is not obvious whether instability of the wake and subsequent vortex street generation occur in superfluids. According to von Kármán's theory [2, 4], a vortex street is expected to be very long-lived in inviscid fluids, once it is created.

In this Letter, by numerically solving the Gross-Pitaevskii (GP) equation, we show that long-lived alternately aligned vortex pairs are formed in the wake of an obstacle potential moving in a Bose-Einstein condensate (BEC), which is similar to the von Kármán vortex street in classical fluids. Mean-field analysis of systems of a BEC with a moving potential has been performed by many authors from the viewpoints of drag force [5, 6], vortex dynamics near the cylinder [7], critical velocity [8], supersonic flows [9, 10], and multicomponent systems [11, 12]. However, vortex street formation was not found in these studies, probably because the parameter region for which a vortex street emerges is narrow, as shown later.

We consider a BEC of atoms with mass $m$ and an obstacle potential $V$ moving in the $-x$ direction at a velocity $v$. In the mean-field theory, the condensate is described by the macroscopic wave function $\psi$ obeying the GP equation given by

$$i\hbar \frac{\partial \psi}{\partial t} = -\frac{\hbar^2}{2m}\nabla^2\psi + V\psi + g|\psi|^2\psi, \tag{1}$$

where $g = 4\pi\hbar^2 a/m$ with $a$ being the $s$-wave scattering length of the atoms. We employ a Gaussian potential with peak strength $V_0$ and radius $d$ moving in the $-x$ direction at a velocity $v$ as $V = V_0 \exp\{-[(x+vt)^2 + y^2]/d^2\}$. Normalizing space and time by $\hbar/(mgn_0)^{1/2}$ and $\hbar/(gn_0)$, where $n_0$ is the atom density far from the potential, we can eliminate the interaction parameter $g$ from Eq. (1). We numerically solve Eq. (1) in two dimensions under the periodic boundary condition using the pseudo-spectral method. The initial state is the stationary state of Eq. (1) with $v = 0$ plus a small amount of noise to break the symmetry.

Figure 1 shows typical wakes flowing past an obstacle potential with $V_0/(gn_0) = 100$. For a sufficiently small velocity $v$, the flow around the obstacle is a steady laminar flow and no quantized vortex is created. When the velocity $v$ exceeds a critical velocity, which depends on the interaction strength and the shape of the potential, vortex-antivortex pairs are created [5]. The critical velocity for the vortex creation is of the order of the speed of sound $(gn_0/m)^{1/2}$. When a created vortex-antivortex pair separates from the potential, the flow velocity around the potential again exceeds the critical velocity and a subsequent vortex-antivortex pair is created. A train of vortex-antivortex pairs is thus generated behind the potential. Since a symmetric double row of vortices is unstable [4], the vortex pairs are dislocated sinuously as shown in Fig. 1 (a). Nore *et al.* [13] showed that such a staggered vortex pattern is formed if a double row of vortices is prepared with an appropriate perturbation. Since a pair of point vortices with circulations $\pm h/m$ ($h$: Planck's constant) and distance $d$ moves in the direction perpendicular to a line between the pair at a velocity $\hbar/(md)$ [4], the alternately inclined vortex pairs move in two directions [white arrows in Fig. 1 (a)], forming a V-shaped wake as in Fig. 1 (a). The divergence of the wake is significant for large $v$, which forms a pattern similar to supersonic flow [9, 10].

Figure 1 (b) shows the main result of this study. The

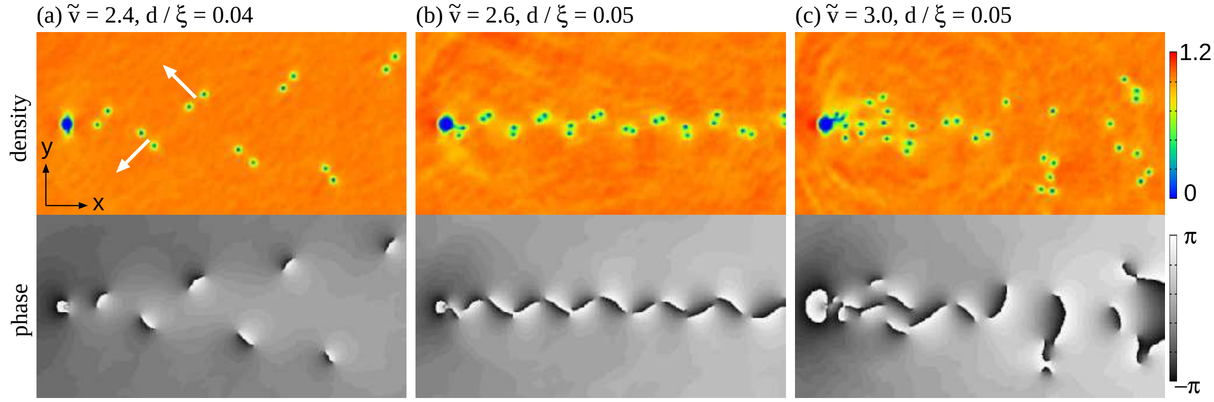



FIG. 1: (Color) Density and phase distributions of a condensate past an obstacle potential. The velocity and potential width are $(\tilde{v}, d/\xi) = (2.4, 0.04)$ in (a), $(2.6, 0.05)$ in (b), and $(3.0, 0.05)$ in (c), where $\tilde{v} = v[10^3 m/(gn_0)]^{1/2}/(2\pi)$ and $\xi = \hbar[10^3/(mgn_0)]^{1/2}$. The white arrows in (a) indicate the directions in which the vortex-antivortex pairs move. The density is normalized by $n_0$. The field of view is $6\xi \times 3\xi$. In the numerical calculation, a $32\xi \times 8\xi$ space is discretized into $4096 \times 1024$.

significant difference from Fig. 1 (a) is that the vortices in a pair created by the obstacle potential at a time have the same circulation. Since two point vortices having the same circulation $h/m$ rotate around their center at an angular frequency $2\hbar/(md^2)$ without changing their distance [4], the created vortex pairs in Fig. 1 (b) remain bound and rotate. The pairs with opposite circulations are alternately released from the obstacle potential to form a train of vortex pairs, resembling a von Kármán vortex street. In contrast to the vortex arrangement originally considered by von Kármán, in which isolated point vortices are aligned, the vortex pairs constitute the vortex street in the present case. We find from Fig. 1 (b) that the distance between the two vortex rows is $b \simeq 0.24\xi$ and the distance between two pairs in a row is $\ell \simeq 0.87\xi$ on average, and hence $b/\ell \simeq 0.28$, where $\xi = \hbar[10^3/(mgn_0)]^{1/2}$. This ratio is in good agreement with the stability condition of von Kármán's vortex arrangement $b/\ell = \pi^{-1} \cosh^{-1} \sqrt{2} \simeq 0.28$ [2, 4]. In fact, the vortex street in Fig. 1 (b) survives at least $t > 10^3\hbar/(gn_0)$. The vortex street in Fig. 1 (b) moves in the $-x$ direction at a velocity $\simeq 0.14(gn_0/m)^{1/2} \simeq 0.8h/(\sqrt{2}\ell m)$. The velocity of von Kármán's point vortices, in which each vortex has a circulation $2h/m$, is $h/(\sqrt{2}\ell m)$ [2, 4]. For large $d$ and $v$, the periodicity in the wake seems to disappear [Fig. 1 (c)]. We have numerically confirmed that similar wakes are also obtained for a disk-shaped potential ($V = \infty$ for $r < d$ and $V = 0$ for $r > d$).

Figure 2 shows the dynamics of vortex street formation just behind the obstacle potential. The pairs of vortices are released obliquely backward left and right with alternate circulations. This vortex street formation behavior is quite different from that in classical viscous fluids, in which a pair of eddies in the wake becomes unstable and grow into a vortex street in the downstream region. In contrast, we find from Fig. 2 that the alternate vortices are directly created at the obstacle, implying that the mechanism of vortex street formation in Fig. 2 may be different from that in classical fluids.

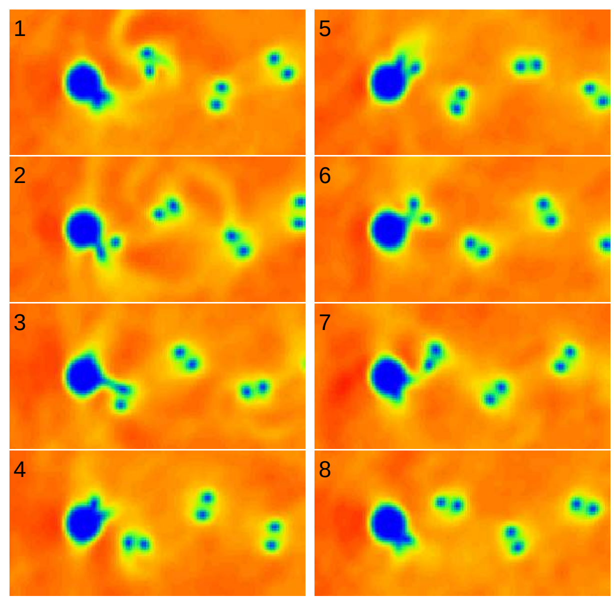



FIG. 2: (Color) Serial snapshots of the density profiles for the parameters in Fig. 1 (b) in the frame moving with the potential. The time interval is $10\hbar/(gn_0)$. The field of view is $2\xi \times \xi$. The color scale is the same as that in Fig. 1.

We systematically performed numerical simulations for various values of $d$ and $v$ to determine the parameter regions for the types of wakes in Fig. 1. Figure 3 shows a rough sketch of each parameter region. The regions of the periodic behaviors shown in Figs. 1 (a) and 1 (b) are located between the regions of steady laminar flow (white region in Fig. 3) and irregular flow (red). We note that the parameter region for vortex street formation is rather restricted, $0.04 \lesssim d/\xi \lesssim 0.13$ and $1.9 \lesssim \tilde{v} \lesssim 2.8$,

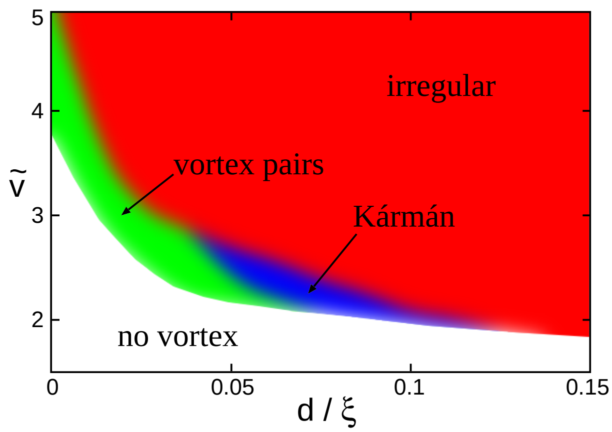



FIG. 3: (Color) Dependence of the patterns of wakes on the normalized Gaussian width $d/\xi$ and velocity $\tilde{v}$ of the potential. The green, blue, and red regions correspond to the flow patterns shown in Figs. 1 (a), 1 (b), and 1 (c), respectively. The white region corresponds to stationary laminar flow.

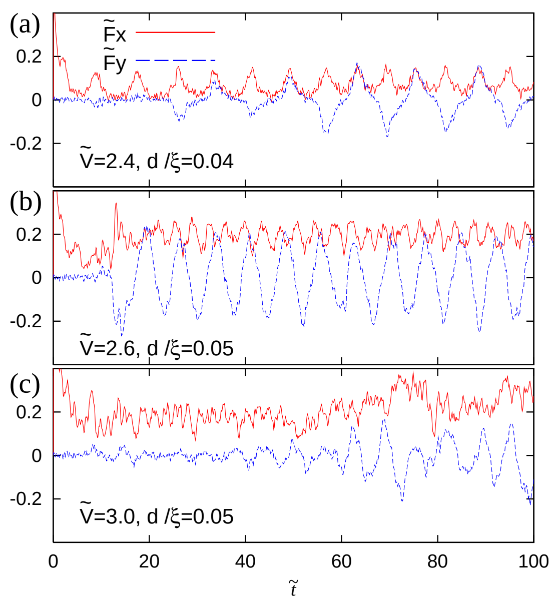



FIG. 4: (Color online) Time evolution of the normalized drag force $\tilde{\boldsymbol{F}} = \boldsymbol{F}\hbar m^{-1/2}(10^{-3}gn_0)^{-3/2}$. The solid and dashed lines show $\tilde{F}_x$ and $\tilde{F}_y$. The parameters used in (a)-(c) are the same as those in Figs. 1 (a)-(c), respectively. Time is normalized as $\tilde{t} = 10^{-3}tgn_0/\hbar$.

where $\tilde{v} = v[10^3 m/(gn_0)]^{1/2}/(2\pi)$. This is in contrast with classical fluids, in which the von Kármán vortex street emerges for a wide range of Reynolds number.

Figure 4 shows the drag force on the obstacle potential given by $\boldsymbol{F} = \partial_t \int d\boldsymbol{r}\psi^*(i\hbar\boldsymbol{\nabla})\psi$. The initial state is the stationary state for $v = 0$. At $t = 0$ the potential starts to move at a velocity $v$. Figure 4 (a) corresponds to the vortex-antivortex pair creation in Fig. 1 (a). For $\tilde{t} \lesssim 20$, $F_x$ oscillates while $F_y \simeq 0$, indicating that the vortex-antivortex pairs are shed from the potential symmetrically. For $\tilde{t} \gtrsim 20$, the vortex pairs begin to incline as in Fig. 1 (a), and $F_y$ also starts to oscillate. Figure 4 (b) corresponds to the vortex street formation, where both $F_x$ and $F_y$ oscillate for $\tilde{t} \gtrsim 20$. The oscillation in $F_y$ in Figs. 4 (a) and 4 (b) is due to the alternate shedding of vortices and hence its frequency is half the vortex shedding frequency, i.e., the frequency of $F_x$. It is interesting to note that $F_y$ in Fig. 4 (c) oscillates, even though Fig. 1 (c) does not seem to have periodicity. A similar phenomenon is also observed in classical fluids with a large Reynolds number [14].

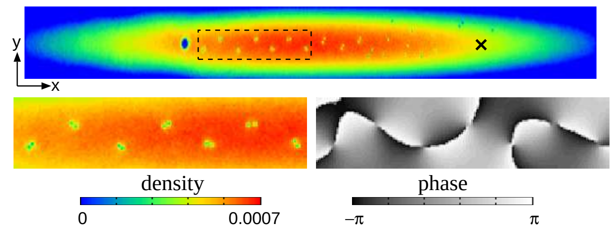



FIG. 5: (Color) Density profile of a BEC of $^{87}$Rb atoms confined in a harmonic potential at $t = 330$ ms. The Gaussian potential is initially located at the marked position ($\times$) and starts to move in the $-x$ direction at a constant velocity. The density and phase profiles in the dashed region are magnified in the lower panels. The field of view is $430 \times 43$ $\mu$m for the main panel and $86 \times 21$ $\mu$m for the lower panels. The color bar is normalized by $Nm\omega_y/\hbar$.

Next, we study a realistic system confined in a trapping potential. A BEC stirred by a moving obstacle potential has been studied experimentally in Refs. [15–17]. We consider a situation in which a BEC of $^{87}$Rb atom is confined in a harmonic potential $m(\omega_x^2 x^2 + \omega_y^2 y^2 + \omega_z^2 z^2)/2$ with $(\omega_x, \omega_y, \omega_z) = 2\pi \times (2.5, 25, 1250)$ Hz. The number of atoms is $N = 10^6$ and the $s$-wave scattering length is $100a_{\rm B}$ with $a_{\rm B}$ being the Bohr radius. The condensate is tightly confined in the $z$ direction and the system is effectively two dimensional. The obstacle potential is produced by a blue-detuned Gaussian laser beam with $d = 2.16$ $\mu$m and $V_0 = 100\hbar\omega_y$, which is initially located at $x = 130$ $\mu$m and $y = 0$ at $t = 0$ and moves in the $-x$ direction at a velocity $v = 0.68$ mm/s for $t > 0$. Figure 5 shows the density and phase profiles at $t = 330$ ms. We find that a vortex street is generated behind the moving potential, as in Fig. 1 (b), which confirms that our finding can be experimentally observed in an inhomogeneous system. The ratio $b/\ell$ in Fig. 5 is about 0.22, which deviates from 0.28 due to the finite size effect.

A future prospect of this study is to provide a mathematical description of the symmetry breaking instability and clarify the mechanism of the alternate creation of the vortex pairs as shown in Fig. 2. In classical viscous fluids, the transition from stationary flow to a vortex street is characterized by the Hopf bifurcation and described by the Stuart-Landau model [18]. A similar approach may

be applied to the present phenomenon. Various shapes of obstacle potentials and three dimensional dynamics also merit further study.

In conclusion, we have shown that pairs of quantized vortices shed from an obstacle potential moving in a BEC alternately align and survive for a long time [Figs. 1 (b) and 2], which closely resembles the von Kármán vortex street in classical fluids. We have obtained the parameter region in which a vortex street emerges (Fig. 3) and calculated the drag force (Fig. 4). We have shown that vortex street formation can be observed in a trapped BEC disturbed by a blue-detuned laser beam (Fig. 5). Since the von Kármán vortex street typifies the great diversity of classical fluid dynamics, the emergence of the von Kármán vortex street in a BEC implies that a rich variety of phenomena is still unrevealed in quantum hydrodynamics.

We thank T. Miyazaki and N. Takahashi for their valuable comments. This work was supported by the Ministry of Education, Culture, Sports, Science and Technology of Japan (Grants-in-Aid for Scientific Research, No. 17071005 and No. 20540388).

[1] H. Bénard, C. R. Acad. Sci. Paris **147**, 839 (1908); **147**, 970 (1908).
[2] T. von Kármán, Nachr. Ges. Wiss. Göttingen, Math. Phys. Kl. 509 (1911); 547 (1912).
[3] For review, see for example, C. H. K. Williamson, Annu. Rev. Fluid Mech. **28**, 477 (1996).
[4] For example, H. Lamb, *Hydrodynamics*, 6th ed. (Dover, New York, 1945), Chap. VII.
[5] T. Frisch, Y. Pomeau, and S. Rica, Phys. Rev. Lett. **69**, 1644 (1992).
[6] T. Winiecki, J. F. McCann, and C. S. Adams, Phys. Rev. Lett. **82**, 5186 (1999).
[7] C. Nore, C. Huepe, and M. E. Brachet, Phys. Rev. Lett. **84**, 2191 (2000).
[8] J. S. Stießberger and W. Zwerger, Phys. Rev. A **62**, 061601(R) (2000).
[9] G. A. El, A. Gammal, and A. M. Kamchatnov, Phys. Rev. Lett. **97**, 180405 (2006).
[10] I. Carusotto, S. X. Hu, L. A. Collins, and A. Smerzi, Phys. Rev. Lett. **97**, 260403 (2006).
[11] H. Susanto, P. G. Kevrekidis, R. Carretero-González, B. A. Malomed, D. J. Frantzeskakis, and A. R. Bishop, Phys. Rev. A **75**, 055601 (2007).
[12] A. S. Rodrigues, P. G. Kevrekidis, R. Carretero-González, D. J. Frantzeskakis, P. Schmelcher, T. J. Alexander, and Yu. S. Kivshar, Phys. Rev. A **79**, 043603 (2009).
[13] C. Nore, M. E. Brachet, and S. Fauve, Physica D **65**, 154 (1993).
[14] A. Roshko, J. Fluid Mech. **10**, 345 (1961).
[15] C. Raman, M. Köhl, R. Onofrio, D. S. Durfee, C. E. Kuklewicz, Z. Hadzibabic, and W. Ketterle, Phys. Rev. Lett. **83**, 2502 (1999).
[16] R. Onofrio, C. Raman, J. M. Vogels, J. R. Abo-Shaeer, A. P. Chikkatur, and W. Ketterle, Phys. Rev. Lett. **85**, 2228 (2000).
[17] T. W. Neely, E. C. Samson, A. S. Bradley, M. J. Davis, and B. P. Anderson, arXiv:0912.3773.
[18] C. Mathis, M. Provansal, and L. Boyer, J. Phys. Paris Lett. **45**, 483 (1984); M. Provansal, C. Mathis, and L. Boyer, J. Fluid Mech. **182**, 1 (1987).